Magnetic nanostructures from block copolymer lithography: Hysteresis, thermal stability, and magnetoresistance

J. Y. Cheng, W. Jung, and C. A. Ross*
Department of Materials Science and Engineering, Massachusetts Institute of Technology, Cambridge, Massachusetts 02139, USA
(Received 21 July 2003; revised manuscript received 21 May 2004; published 26 August 2004)

A series of two dimensional close-packed Co, NiFe, and CoFe/Cu/NiFe magnetic particle arrays, in which the particles have mean diameters of 34 nm, thicknesses of 5–20 nm, and periodicity of 56 nm, were made using a process based on self-assembled polystyrene-*b*-polyferrocenyldimethylsilane block copolymer templates. Interparticle magnetostatic interactions lead to the thermally assisted collective reversal of small groups of particles. The switching field distribution, whose width decreases as the thickness increases, has been modeled as a result of the distribution of particle size, shape, and microstructure. For multilayered particles, interlayer magnetostatic interactions stabilize flux-closed states with antiparallel alignment of the CoFe and NiFe layers at remanence. The multilayer particles show a greater thermal stability than single-layer particles, and a magnetoresistance comparable to that of the unpatterned film.

DOI: 10.1103/PhysRevB.70.064417 PACS number(s): 75.75.+a, 75.47.−m, 83.80.Uv, 81.16.Nd

I. INTRODUCTION

The behavior of arrays of nanoscale magnetic particles is interesting both from a fundamental point of view, and also for applications in magnetic recording media, magnetic cellular automata, or magnetoelectronic devices. Recent advances in nanofabrication technology have made possible the study of magnetic particles with dimensions of order 10 nm and above.[1,2] In the sub-100-nm regime, magnetic particles are single-domain (or nearly so) at remanence, but reversal typically occurs nonuniformly,[3] and the reversal is thermally assisted. For sufficiently small magnetic anisotropy energy K and particle volume V, i.e., for $KV < 25k_BT$ for an isolated particle, superparamagnetic behavior is observed (where k_B is Boltzmann's constant and T the temperature).[4,5] Measurements of particle arrays invariably reveal a spread in the switching fields of nominally identical particles [for example, Refs. 6–9]. This switching field distribution has been attributed to surface anisotropy, differences in size and shape, or microstructural variability between the particles, and is found even in particles patterned from single crystal films.[10–12] Additionally, for closely spaced particles, magnetostatic interactions influence the behavior of the array by stabilizing certain configurations of the magnetic moments of neighboring particles. This can sharpen or broaden the switching field distribution, depending on the arrangement of the particles in the array.[13,14]

To identify the effects of these factors on magnetic behavior, there have been extensive studies of planar arrays of magnetic particles fabricated using nanolithography, in particular using electron-beam lithography. This method has a spatial resolution of order 10 nm, and the ability to define arbitrary shaped patterns, but its relatively low throughput limits the area of the structures that can be made. Alternative methods have therefore been developed that can pattern large areas with identical periodic structures. These methods can be based on optical interference,[3,6,15–17] which produces patterns with long-range coherence, or on self-assembling systems, which generally produce high-density patterns with only short-range order. Two-dimensional arrays of nanoparticles, nanowires, and antidots (holes) have been made using self-assembled anodized alumina,[18–23] colloidal crystals,[24] and block copolymers[25–36] as templates. Magnetic arrays can also be made directly by the self-assembly of nanoparticles formed by solution chemistry.[37] The present work is based on block copolymer lithography, where phase separation within a thin film of a block copolymer generates a periodic array that can be used as a template to pattern arrays of nanoscale structures.

Methods based on block copolymer templates are attractive because the process can be integrated with more conventional semiconductor processing methods,[35,38] and because the size and morphology of the template can be selected by choosing the molecular weight and composition of the polymer. Long-range order can also be induced in block copolymer films by the use of topographically[39–41] or chemically[42] patterned substrates or by electric fields.[43] We have demonstrated that organic-organometallic polystyrene-*b*-polyferrocenyldimethylsilane (PS-PFS) block copolymers can be used to make an etch mask for patterning of silica, and the silica pattern can then be transferred into a range of other materials.[31,32] Other groups have used organic block copolymers such as polystyrene-*b*-polymethylmethacrylate for templating arrays of parallel Co or Ni wires made by electrodeposition.[25,30] Previous work on thin film structures made by block copolymer lithography has included a study of exchange bias and anisotropic magnetoresistance in Fe antidot arrays (network structures),[26] and a study of hysteresis in perpendicularly magnetized CoCrPt particles.[34] However, some of the key attributes of these arrays have not been explored. In particular, the thermal stability, interactions, and the origins of variability of properties within arrays, and the behavior of particle arrays patterned from multilayer films, have not been described. These attributes are important for applications such as patterned magnetic media, semiconductor memories[35] or other devices that incorporate nanostructures.

This paper presents a detailed study of the magnetic properties of single layer Co and $Ni_{80}Fe_{20}$ (permalloy) particles

and multilayer particles of a $Co_{84}Fe_{16}/Cu/Ni_{80}Fe_{20}$ pseudo-spin-valve structure made using PS-PFS block copolymer templates with 56 nm periodicity. Data from time-dependent coercivity measurements and ΔM curves are related to the reversal process and the nature of interactions between the particles in the arrays. The switching field distributions are analyzed in terms of the deviation of the particle shapes from perfect cylinders and the polycrystallinity of the films from which the particles are made. In the case of pseudo-spin-valve particles, both hysteresis and magnetotransport show that the patterning process preserves the multilayer structure and magnetoresistance of the film.

II. EXPERIMENTAL METHODS

Samples were made using block copolymer lithography in a process described elsewhere.[31,32] Films of Co and $Ni_{80}Fe_{20}$ with thicknesses of 5, 10, 15, and 20 nm were deposited onto oxidized silicon wafers by electron-beam evaporation with a base pressure in the mid-10^{-7} Torr range. Multilayer films consisting of 3.3 nm $Co_{84}Fe_{16}$/6.0 nm Cu/4.5 nm $Ni_{80}Fe_{20}$ pseudo-spin-valve (PSV) structures were sputtered in an UHV chamber with a base pressure in the 10^{-9} Torr range, at 1 mTorr sputter pressure, and 6 W/cm^2 sputter power. The alloy compositions are given in at. %, and will be referred to subsequently as NiFe and CoFe for brevity. The magnetic films were coated with a pattern transfer layer consisting of 20 nm W followed by 50 nm silicon oxide, deposited using electron-beam evaporation. Finally, a solution of polystyrene-*b*-polyferrocenyldimethylsilane (PS-PFS) with molecular weights of 91 k for the PS and 21 k for the PFS was spin-cast at 2000 rpm onto the SiO_2/W/magnetic stack. The samples were then annealed at 180°C for 48 h to cause spontaneous phase separation in the polymer film, forming a close-packed monolayer of PFS spheres embedded in a 50 nm thick PS matrix. Four successive reactive ion etching (RIE) processes were used to remove the PS matrix (O_2 gas), to transfer the PFS sphere pattern into the oxide (CHF_3 gas), to transfer the oxide pattern into the W hard mask layer (CF_4+O_2 gas), then to remove residual polymer and silica (high pressure CHF_3 gas). Finally, arrays of discrete magnetic particles were produced by ion-beam etching the magnetic film in a neon plasma, using the W as a hard mask. Use of Ne provides optimum selectivity between the mask and magnetic films. It is possible to remove the remaining W by reactive ion etching, but in these experiments it was left covering the magnetic particles to provide partial protection from oxidation.

This process leads to close-packed arrays of circular thin-film magnetic elements over areas of 1 cm^2 or greater. The periodicity (center-to-center spacing) of the arrays was 56 nm with a standard deviation of 3.3 nm, and the particle diameter was 34 nm, so there is a gap of at least 22 nm between adjacent particles. The periodicity corresponds to 4.3×10^{10} magnetic particles cm^{-2}, and is determined by the molecular weight of the PS-PFS polymer chains. The molecular weight of the minority PFS block determines the diameter of the particles, although this can be modified slightly by the etching conditions. Examples of Co arrays of different thickness are shown in Fig. 1. Slightly tapered sidewalls are observed in the thicker sample due to the faceting effect of longer ion-beam etching time.

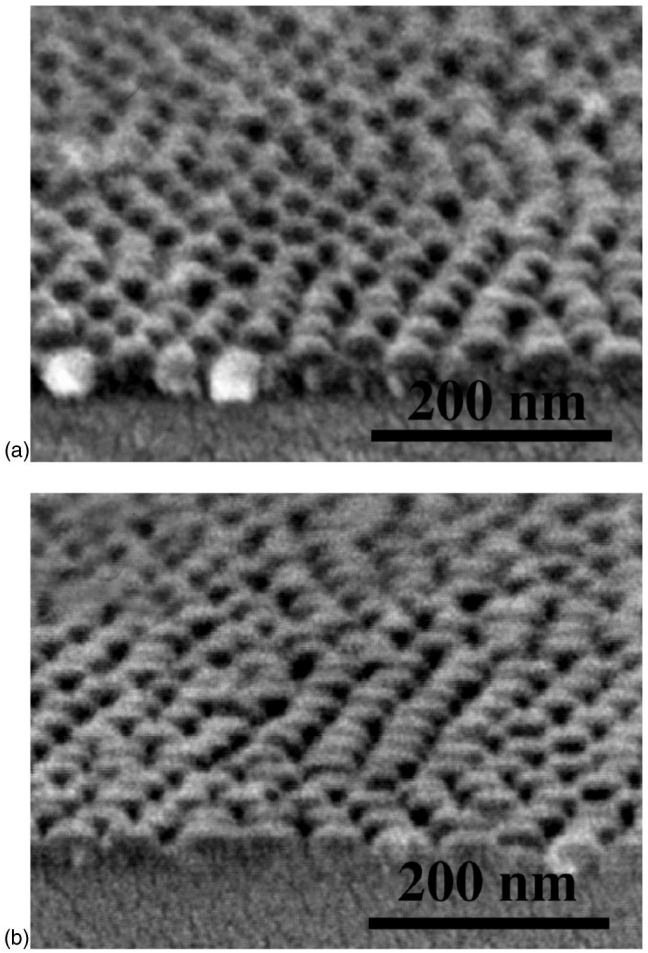

FIG. 1. Tilted SEM cross-section micrographs of (a) a 15 nm nm thick Co array; and (b) a 5 nm thick Co array. The magnetic particles appear taller than the Co film thickness due to the presence of a residual W layer capping each particle.

The magnetic hysteresis of the Co, NiFe, and PSV arrays were measured using a vibrating sample magnetometer (VSM) and an alternating gradient magnetometer (AGM) at room temperature in ambient atmosphere. The gradient field for the AGM measurement was 1 Oe and the sweep rate was varied from 0.1 to 100 Oe/s. The normalized switching field distribution (SFD) was calculated from the full width at half maximum of the derivative of the hysteresis loops, fitted to a Gaussian function, divided by the coercivity. The switching volume (activation volume) of the arrays, V_S, was determined by measuring the scan-rate dependence of the coercivity.[44–47] The measured coercivity $H_C(t)$ is related to the measurement time t according to:[44]

$$H_C(t) = H_0\{1 - [(k_BT/K_{\text{eff}}V_S)\ln(0.69f_ot)]^n\}, \qquad (1)$$

where f_o is an attempt frequency taken as 10^9 s^{-1},[44] and H_0 is the coercivity measured in the limit of high scan rates. H_0 is given by $2K_{\text{eff}}/M_s$ where K_{eff} is the net magnetic anisotropy and M_s the saturation magnetization. This derivation is

based on the assumption of a population of noninteracting uniaxial particles with their easy axes parallel to the applied field. The value of n is 0.5 for ideal Stoner-Wohlfarth reversal, but for particles with a distribution of orientations and activation energies, and in the presence of interactions, higher values for n are found to give a better fit to experimental[44,45] or micromagnetic[46] data. Taking $n=1$, and expressing the measurement time as being inversely proportional to the field scan rate $R(\mathrm{Oe/s})$ during the hysteresis loop measurement, Eq. (1) can be rewritten in the form:

$$H_C(R) = C + (k_B T/M_S V_S)\ln(R), \qquad (2)$$

where C is a constant. By equating t with the field step time during the measurement, K_{eff} can be found, and the energy barrier for magnetization reversal was then calculated as $K_{\mathrm{eff}}V_S$. The absolute values of switching volume will depend on the parameters (n, f_o) chosen for the fitting procedure,[44] but the trends in switching volume with particle thickness are irrespective of the exact form of $H_C(R)$.

The interactions between the magnetic particles were characterized by comparing their isothermal remanent magnetization (IRM) and dc demagnetization (DCD) curves.[48,49] The IRM curve was obtained by magnetizing an initially ac-demagnetized sample by applying an increasing field, H, in small steps and measuring the remanence, $M_r(H)$, after removal of the field. The DCD curve was similarly measured by applying an increasing positive field to an initially negatively saturated sample, and measuring the remanence, $M_d(H)$, after removal of the field. The ΔM, which is defined as

$$\Delta M(H) = M_d(H)/M_r(\infty) - [1 - 2M_r(H)/M_r(\infty)], \qquad (3)$$

characterizes the deviation of the sample from a system of noninteracting particles. For an ensemble of non-interacting Stoner-Wohlfarth particles, ΔM is exactly zero for all H. A negative ΔM indicates that DCD falls more rapidly with field than 2IRM, i.e., the interactions between particles initially assist in reversal and promote demagnetization of the ensemble, while positive ΔM indicates that interactions initially impede reversal and stabilize the magnetized state.

Magnetotransport measurements were made on the array of PSV particles after coating it with 5 nm evaporated Au. Measurements were done using a four-point probe with an in-plane applied magnetic field. The giant magnetoresistance (GMR) ratio was defined as $[\rho(H)/\rho(H_{\max})-1]\times 100\%$, where ρ is the resistivity, H the applied field, and $H_{\max}=10$ kOe.

X-ray diffraction was used to examine the crystallographic texture of the films and indicated that the Co films are predominantly h.c.p. with a random crystallographic texture and a grain size of order 10 nm. Measurements of the distribution of the geometry of the particles were based on scanning electron micrographs. The micrograph was converted to binary data with an intensity threshold value which defined the boundaries and areas of the particles. Each particle shape was fitted to an elliptical shape and the two principal axes were measured.

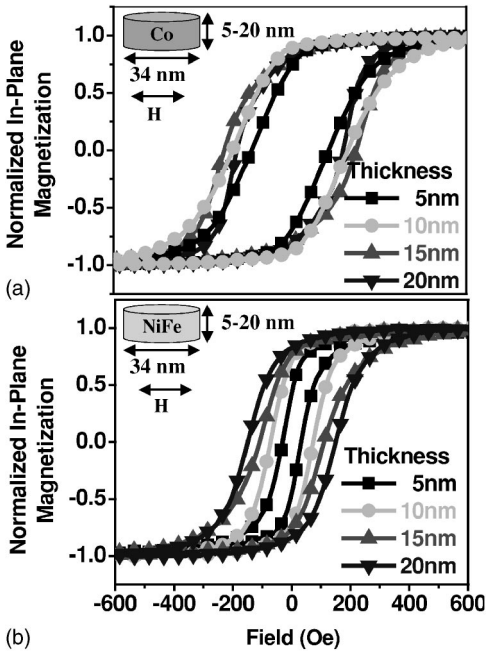

FIG. 2. The in-plane hysteresis loops of single-layer (a) Co arrays and, (b) NiFe arrays with thicknesses of 5, 10, 15, and 20 nm. The moment is normalized to the saturation magnetization of each sample.

The two-dimensional NIST Object Oriented Micromagnetic Framework (OOMMF) Program was employed to simulate the magnetization reversal process of single-layer Co and NiFe elements. An elliptical or circular particle was discretized into 4 nm cells, which results in edge roughness of up to 4 nm. A 3D-random orientation of the magnetocrystalline easy axis was assigned to each cell to represent the 3D-random polycrystallinity of the particle. Hysteresis loops and remanence states were generated for individual circular (36 nm diameter) and low aspect ratio elliptical (36 nm $\times$ 32 nm) particles with thickness of 4 or 20 nm, made from either NiFe or Co. For the elliptical particle the field was applied along the long axis. Multiple calculations were made for each geometry or material, with a different random distribution of magnetocrystalline easy axes in each calculation, to simulate the effects of the polycrystallinity on the switching field distribution. Standard parameters for Co (exchange stiffness $A=3\times10^{-6}$ erg cm^{-1}, saturation moment $M_s=1420$ emu cm^{-3}, uniaxial magnetocrystalline anisotropy, $K_u=5.2\times10^6$ erg cm^{-3}) and NiFe ($A=1.3\times10-^{6}$ erg cm^{-1}, $M_s=800$ emu cm^{-3}, cubic anisotropy, $K_1=5\times10^3$ erg cm^{-3}) were used, and the damping coefficient was set to 0.5.

III. RESULTS

At remanence, the unpatterned Co and NiFe films were magnetized in-plane. The coercivities were 8–18 Oe for Co, and 5–14 Oe for NiFe, increasing with thickness. Patterning increased the coercivity considerably, up to 228 Oe for Co arrays and 160 Oe for NiFe arrays. The coercivity typically increased with particle thickness as shown in Figs. 2 and 3. All the arrays have an in-plane easy axis. The in-plane loops

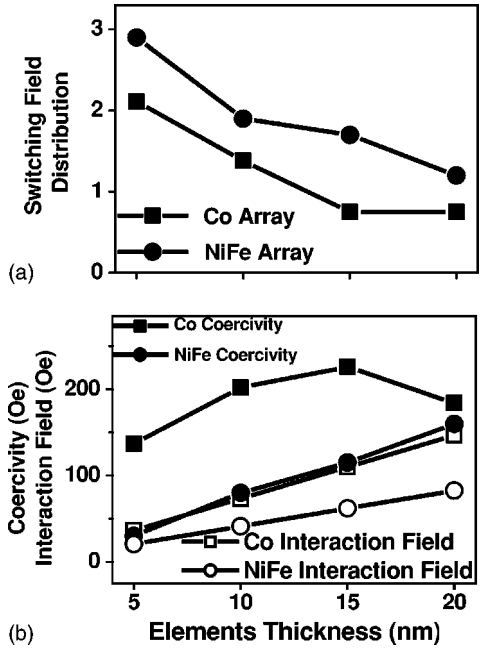

FIG. 3. (a) Switching field distribution of Co and NiFe arrays, calculated as the full width at half maximum of the field derivative of the hysteresis loop, divided by the coercivity. (b) The coercivity of the Co and NiFe arrays (solid symbols) and the calculated interaction field between a pair of neighboring particles (open symbols).

of Co and NiFe particles show a wide switching field distribution (defined above) varying from 0.8 to 2.9. Figure 3(a) shows that the SFD decreases with increasing thickness, and is higher for NiFe than for Co. In contrast, the out-of-plane loops have low remanence and saturate at fields of 8–12 kOe in the case of Co.[32]

Figure 4 shows linear least-squares fits to the data for coercivity versus the logarithm of the field scan rate. The higher slope of the fit line for thinner arrays indicates that the switching volume for thermally assisted magnetization reversal decreases with decreasing film thickness. The switching volume V_S calculated for the in-plane magnetization reversal process from Eq. (2) is compared to the physical volume V_P of the particles in Fig. 5(a). The ratio of V_S/V_P is 2–6 for NiFe arrays and 1.5 for Co arrays. Figure 5(b) plots the energy barrier for reversal in the samples. These data give values for K_{eff} of 3×10^5–4×10^5 erg/cm^3 for the Co arrays and 7×10^3–1.5×10^4 erg/cm^3 for the NiFe arrays. It is worth emphasizing that the strong interactions between the particles, and the lack of uniaxial anisotropy, contradict the assumptions behind Eq. (2), but the calculated switching volumes nonetheless give a qualitative indication of the reversal process.

The results of a ΔM measurement on two Co arrays are shown in Fig. 6. The interactions are stronger, relatively, in the 5 nm thick array compared to the 15 nm thick array. The negative ΔM indicates that reversal occurs at lower fields if the sample starts from a dc demagnetized state compared to an ac demagnetized state, i.e., the ac demagnetized state is more stable and has a higher reversal field.

Figure 7 shows hysteresis loops and MR curves for both the patterned and unpatterned CoFe/Cu/NiFe multilayer

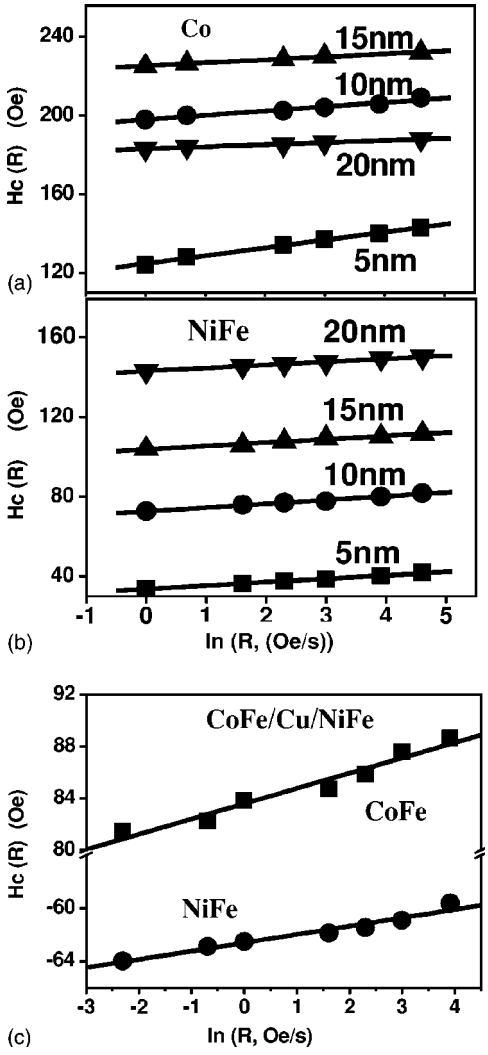

FIG. 4. Scan-rate dependent coercivity with linear fits for (a) Co, (b) NiFe, and (c) CoFe/Cu/NiFe arrays. R is the field scan rate in Oe/s. The data for the thinner arrays have a larger slope indicating a smaller switching volume.

film. The two multilayer films were grown in separate batches using the same deposition conditions. There are two distinct steps in the hysteresis loops, although the patterned film shows a much greater SFD. In the unpatterned film the NiFe layer and the CoFe layer switch at fields of 5 and 21 Oe, respectively, and the two layers are magnetized parallel at remanence. In contrast, the hysteresis loop for the array shows the hard layer switching at 85 Oe and the soft layer switching at −65 Oe, i.e., the layers in the particles are coupled antiparallel at remanence. The magnetotransport measurements follow the hysteresis curves of the film and array. The GMR of the Au-coated patterned PSV array was 0.16%, compared to the unpatterned PSV film, which has a GMR of 1.5% (without Au coating). The magnetoresistance of the patterned structure is attributed to GMR and not to anisotropic magnetoresistance, because similar results were obtained irrespective of the angle between the field and the current.

From the data in Fig. 4(c) and Eq. (2) the switching volumes of the CoFe layer and NiFe layer were 2×10^4 and

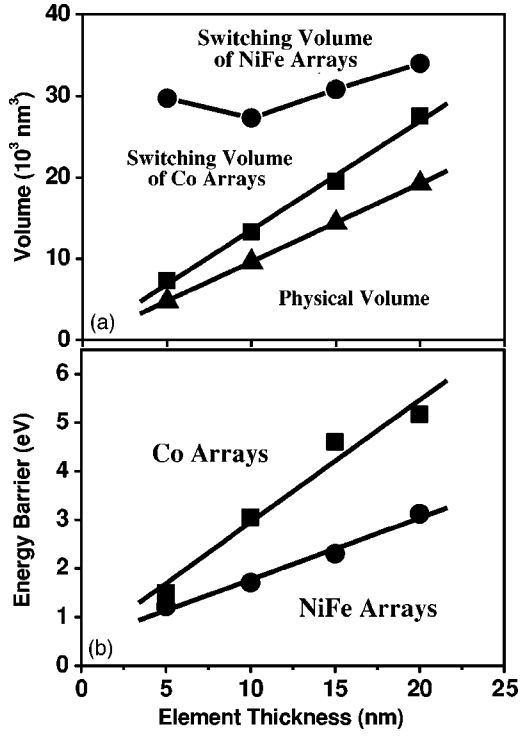

FIG. 5. (a) Comparison of the switching volume and physical volume of the Co and NiFe arrays. The switching volume is larger than the physical volume of the particles, indicating that the particles reverse cooperatively; (b) the energy barrier for reversal in Co and NiFe arrays.

8×10^4 nm^3, respectively, which compared with the physical volumes of 2.5×10^3 and 4.5×10^3 nm^3 show that the ratio of V_S/V_P is 8 for the NiFe and 18 for the CoFe layers.

The particles in the arrays exhibit a distribution in size and shape. A plan-view scanning electron micrograph of an array of 15 nm thick Co particles is shown in Fig. 8(a), which is typical of all the arrays. The particles are locally close packed but the array lacks long-range order, and there is a distribution of diameters, in-plane aspect ratios (ellipticities) and in-plane orientations of the major axis. Statistical results from analyzing 400 magnetic particles from this array are shown in Figs. 8(b) and 8(c). The distribution of ellipticities (defined as the ratio of the major axis length to the minor axis length) is shown in Fig. 8(b). The average ellipticity of the particles is 1.06, and 80% of the particles have ellipticities between 1 and 1.15. The area distribution of the particles is shown in Fig. 8(c). The mean area of each particle is 903 nm^2, which corresponds to the area of a circle of 34 nm diameter. The standard deviation of the diameter is 9%.

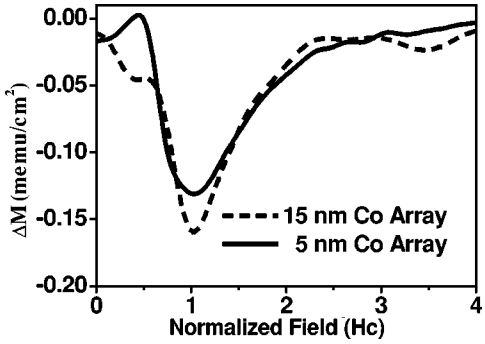

FIG. 6. ΔM plots of 5 and 15 nm thick Co arrays. The applied field is normalized to the coercivity of the samples, which are 140 and 228 Oe, respectively.

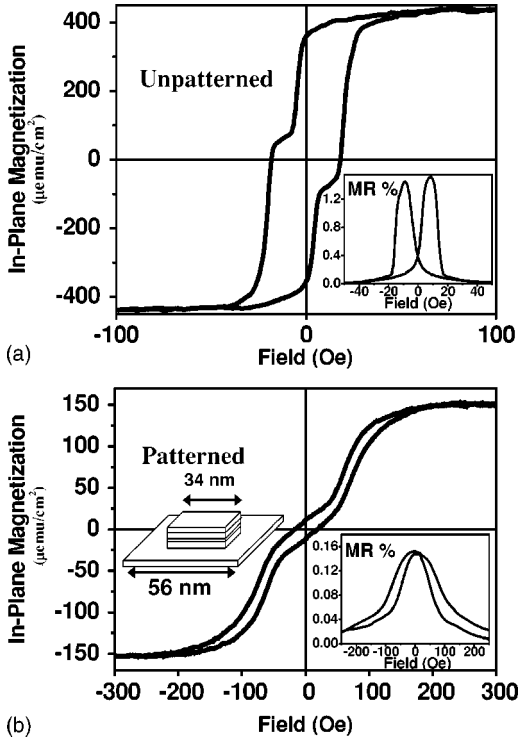

FIG. 7. Hysteresis loops of (a) unpatterned CoFe/Cu/NiFe PSV film, and (b) patterned PSV array after coating with 5 nm Au. The insets show the corresponding magnetoresistance data. The schematic in (b) illustrates how the array was electrically modeled as an array of unit cells, each of which consisted of a 34 nm diameter, 13.8 nm thick PSV element with a 20 nm W cap on a 56 nm diameter, 5 nm thick Au shunt layer.

Figure 9 shows the results of repeated OOMMF simulations of 36 nm$\times$32 nm elliptical magnetic particles. About 40 simulations were carried out for each of four types of particle: NiFe with thickness of 4 and 20 nm, and Co with thickness of 4 and 20 nm. In each set of 40 simulations the geometry was unchanged but the 3D orientation of the magnetocrystalline anisotropy in each 4 nm cell was randomly reassigned. The range of behavior of the simulations therefore gives a qualitative indication of the influence of the varying magnetocrystalline anisotropy of the polycrystalline particles. Figure 9 shows that there is a distribution of switching fields in each case. To facilitate comparison, the distributions have been normalized to the mean switching field, which was 184 and 374 Oe for 4 nm thick and 20 nm thick Co elements and 30 and 80 Oe for 4 and 20 nm thick NiFe elements, respectively. The Co particles have considerably higher switching fields than NiFe, and thicker particles have higher switching field than thinner particles, as observed experimentally. The thinner particles also have a broader range of switching fields. Remanent states (not

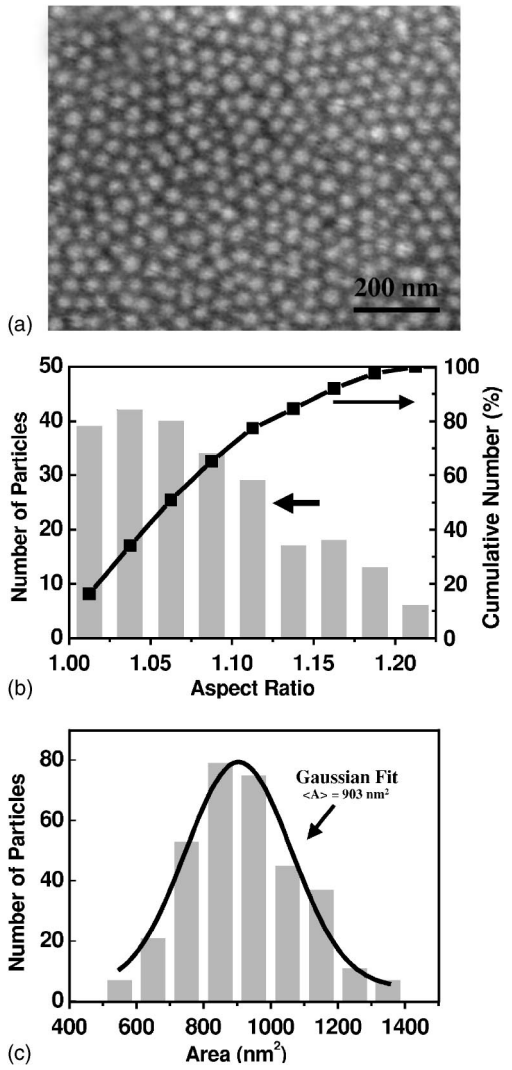

FIG. 8. (a) Plan-view SEM micrograph of a 15 nm thick Co array; (b) the distribution of the in-plane aspect ratios (ellipticities) of the particles; (c) the size distribution of the particles.

shown) also exhibit a variety of configurations; in many cases the remanent state was approximately uniform but was tilted away from the easy axis as a result of the net magnetocrystalline anisotropy.

IV. DISCUSSION

The properties of the arrays are determined both by the behavior of individual particles and by the geometry of the array which defines the magnetostatic interactions between the particles. In all of these samples the magnetization is oriented in plane as a result of shape anisotropy. The magnetic particles are cylindrical with a maximum height/diameter ratio ranging between 0.15 and 0.59, which is less than the value of 0.9 at which the magnetization in a uniformly magnetized cylinder reorients from in-plane to out-of-plane.[50,51] Moreover, the diameter and thickness of the particles are sufficiently small that the particles are expected to exhibit an in-plane uniform (flower-state) magnetization in preference to a flux-closed or "vortex" state,[15,52,53] i.e., the particles ideally approximate in-plane dipoles with zero in-plane coercivity. (The 20 nm thick Co particles are near the flower-vortex boundary,[15] and they may be thick enough to support vortex states.)

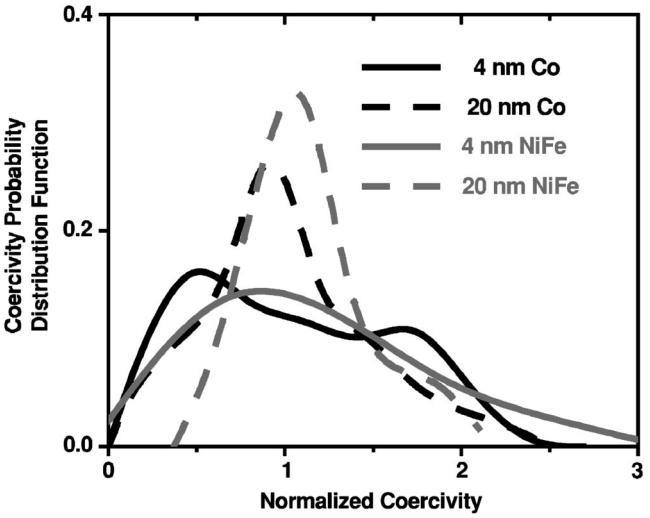

FIG. 9. Coercivity probability distribution based on results of repeated OOMMF simulations for 4 nm thick and 20 nm thick 32 $\times$ 36 nm Co and NiFe particles. For each type of particle, the simulation was repeated about 40 times, each time with a different random distribution of magnetocrystalline anisotropy directions within the 4 nm $\times$ 4 nm cells. The coercivity distribution obtained from the multiple simulations is normalized on the x axis to the average coercivity of the particles, which was 30 Oe for 4 nm thick NiFe, 80 Oe for 20 nm thick NiFe, 184 Oe for 4 nm thick Co, and 374 Oe for 20 nm thick Co. The probability distributions are normalized so that each has an area of 1.

Magnetostatic interactions play a major role in determining the behavior of these closely spaced arrays. In Fig. 3(b), the interaction field between two nearest neighbor particles (calculated using a dipole approximation) is plotted for comparison with the coercivity of the array. The dipole approximation underestimates the interaction field between single domain disks by about 10% for the geometry of our samples.[54] These interactions profoundly affect the reversal process, the in-plane coercivity, and the switching field distribution. The samples may be modeled as hexagonally close packed arrays of dipoles with in-plane magnetization. Simulations[54] indicate that magnetostatic interactions in a hexagonal array lead to the formation of frustrated micromagnetic states where the orientations of adjacent particles' moments are correlated and form closed loops or spirals. As a result of magnetostatic interactions, the in-plane coercivity is nonzero. The coercivity has been calculated for square arrays of in-plane dipoles[55,56] and hexagonal arrays of uniaxial nanoparticles,[57,58] and can be large for closely spaced particles. For example the coercivity reaches $0.1(4\pi M_s)$ for a square array of in-plane dipoles with diameter/period of 0.9,[56] but decreases for more widely spaced particles.

The effect of magnetostatic interactions is also seen in the ΔM data. The IRM measurement starts from an ac-

demagnetized state, in which the particle moments are assumed to be arranged in in-plane flux-closed loops as noted above.[54] A higher field is required to reverse the magnetization in this micromagnetic structure compared to reversing the dc-demagnetized remanent configuration. This inequality leads to a negative ΔM, which is larger for the thinner Co sample because the ratio of interaction field to coercivity is greater. This resembles other systems dominated by magnetostatic interactions, which are characterized by negative ΔM. Additionally, magnetostatic interactions are responsible for the high values of switching volume derived from thermal stability data. The switching volume is greater than the physical volume, particularly for the NiFe arrays, which indicates cooperative reversal of several particles. In contrast, measurements on weakly interacting 30-nm-diameter particles and other small particle systems indicate that the reversal process of isolated particles is incoherent and typically involves a fraction of the volume of the particle.[3,59]

For device applications, one of the most important characteristics of an array of nanomagnets is the switching field distribution. There are several sources of intrinsic variability between nominally identical particles: nonideal shape (ellipticity), variations in size and in the long axis direction, the effects of magnetocrystalline anisotropy in polycrystalline materials, and surface anisotropies. Additionally, the interactions between particles increase the switching field distribution because the local field experienced by each particle is affected by the orientation of its neighbors.

The effects of shape on coercivity can be estimated by considering the shape anisotropy of a triaxial ellipsoid of Co or NiFe with two major in-plane axes of 33 and 35 nm [i.e., the ellipticity is 1.06, as suggested from Fig. 8(b)] and an out-of-plane axis which equals 5, 10, 15, or 20 nm. An in-plane coercivity ranging between 145 Oe for a 5 nm thick Co ellipsoid and 345 Oe for a 20 nm thick Co ellipsoid, and 80 Oe for a 5 nm thick NiFe ellipsoid and 196 Oe for a 20 nm thick NiFe ellipsoid is predicted. These values show that a few percent ellipticity in the particle shape can give rise to a significant in-plane coercivity. Thus, the presence of a small ellipticity can explain the increase in coercivity with increasing thickness, and contributes to the higher coercivity measured for the Co compared to the NiFe.

A further contribution to switching field distribution arises from the variation in area of the particles. A switching field distribution of 0.4–0.5 would be expected for an ensemble of ellipsoidal particles with sizes and shapes as shown in Fig. 8. The ellipticity, as well as the variation of the particle area seen in Fig. 8(c) is also present in SEM images of the block copolymer template, and is believed to originate from the low diffusivity of polymer molecules during annealing, which limits the monodispersity of the PFS spherical domains.

Magnetocrystalline anisotropy contributes to the coercivity and switching field distribution of the particles, particularly the Co arrays. The evaporated magnetic films are polycrystalline with a grain size of order 10 nm (based on electron microscopy of similar films and x-ray diffraction), so each particle contains several grains and the net magnetocrystalline anisotropy is unlikely to be exactly zero. This leads to a nonzero in-plane coercivity even for perfectly cylindrical particles. The effects are evident from the OOMMF simulations on Co and NiFe particles, and have also been estimated statistically in polycrystalline Co.[9,60,61] When repeated OOMMF simulations are performed, in which the 3D distribution of the magnetocrystalline anisotropy is reassigned randomly each time, a distribution of remanent states and coercivities is obtained, as shown in Fig. 9. The switching field distribution (calculated as the full width at half maximum of the distribution divided by the average switching field, from the micromagnetic simulation data) is 1.4 and 1.0 for 4 and 20 nm thick Co particles, and 1.3 and 0.8 for 4 and 20 nm thick NiFe particles. The calculated SFDs decrease with film thickness, as seen experimentally. This modeling treats the grains as squares, 4 nm in lateral dimensions, whereas in the actual samples the grains are larger than 4 nm and the SFD will therefore be higher than the values calculated here.

The thermal activation measurements gave values for the effective anisotropy K_{eff} of the switching volume which is much smaller than the magnetocrystalline anisotropy for both Co and NiFe. K_{eff} includes contributions both from the shape anisotropy and the averaged magnetocrystalline anisotropy of the grains within the particles. K_{eff} has the same order of magnitude as the effective anisotropy given by $H_c M_s/2$, where H_c is determined from the OOMMF modeling (Fig. 9). The energy barrier for reversal is linear with film thickness for both Co and NiFe [Fig. 5(b)]. All the samples have an energy barrier larger than 25 $k_B T$ and are thermally stable at room temperature. However, arrays below $\sim 2-3$ nm thickness are predicted to be superparamagnetic at room temperature.

The preceding discussion suggests that the combined effects of ellipticity, size variations, magnetocrystalline anisotropy from the polycrystalline microstructure, and magnetostatic interactions are sufficient to explain the values of coercivity and the switching field distributions measured for the Co and NiFe particle arrays. Edge roughness, though not quantified in this work, can also pin the magnetization as it rotates and contribute to the coercivity and SFD. The switching field distributions calculated as a result of crystalline anisotropy and ellipticity may be compared with the measured values of 2.1 and 0.8 for 5 and 20 nm thick Co and 2.9 and 1.2 for 5 and 20 nm thick NiFe.

The multilayer nanostructures will now be discussed. The most prominent feature of the hysteresis loop of the PSV array is that the reversal of the soft NiFe layer occurs before zero field, so that the hard and soft layers are magnetized antiparallel at remanence [Fig. 7(b)]. Similar behavior has been seen for other low aspect ratio (width/length) multilayer thin-film elements and is a result of magnetostatic coupling between the hard and soft layers within each particle to give a flux-closed configuration at remanence.[62] The hysteresis behavior is reflected in the magnetoresistance data, where the high-resistance antiparallel state is present at zero field. Although the GMR ratio of the PSV array is small compared to the unpatterned film, this difference can be attributed primarily to the shunting effect of the Au and residual W. An estimate of the expected magnetoresistance of the patterned array can be obtained by approximating the array as consisting of 56×56 nm unit cells in the plane of the substrate.

Each unit cell is modeled as a 34×34 nm CoFe/Cu/NiFe/W particle connected in parallel with a 56 $\times$ 56 nm Au layer. A sketch of the unit cell is shown in Fig. 7(b). Bulk resistivities of the metals were assumed.[63] Based on this estimate, if the uncoated PSV film has a GMR of 1.5%, the GMR of the Au-coated array is predicted to be 0.22% as a result of shunting of the current into the Au and W. This is comparable to the measured value of 0.16% for the Au-coated array, and indicates that the GMR of the patterned elements is within a factor of 0.7 of that of the original film. This result suggests that the patterning process does not significantly degrade the layered structure, in comparison to earlier work on PSV wires.[64]

The behavior of the multilayer array is also strongly affected by interparticle interactions: the nearest-neighbor magnetostatic coupling between two saturated particles is about half of the coercivity of the hard layer. This is supported by the switching volume measurements, which give a value of V^* considerably higher than the physical volume of the magnetic layers. The results suggest cooperative reversal of a number of particles. Indeed, the interactions stabilize the magnetic layers against superparamagnetism, which might be expected in the 3.3 nm thick CoFe layer, which is only slightly thicker than the thickness at which superparamagnetism would occur in single layer Co particles at room temperature.

This work has shown that the magnetic behavior of nanostructure arrays made using block-copolymer lithography can be understood by considering the properties of the individual particles, which vary according to their size, shape, and microstructure, and the geometry of the array which governs magnetostatic interactions between the particles. Micromagnetic simulations substantiate the influence of microstructure on the switching field and the uniformity of the remanent state. The strong magnetostatic interactions in these arrays make them unsuitable for applications such as patterned media, where the particles must reverse independently. To reduce the interaction between particles, arrays with smaller diameter and wider spacing may be produced by using a block copolymer with a smaller volume fraction of the minority PFS phase. A narrower switching field distribution can be achieved by reducing the variation among the particles, for instance by using a single-crystal magnetic film, and improving the uniformity of the block copolymer templates and lowering the edge roughness during patterning. The hysteresis and magnetoresistance of the multilayer particles, whose properties are relevant in the design of deep-submicron magnetoelectronic devices,[65] can be adjusted by varying the layer sequence, for instance the magnetostatic interactions between the hard and soft layers may be reduced by the use of a synthetic antiferromagnet stack.[66] Additionally, long-range ordering of the arrays is possible by templating the self-assembly of the block copolymer, leading to arrays of nanoparticles on the substrate surface with two-dimensional order.[39,40]

V. CONCLUSIONS

Arrays of 34 nm diameter, 5–20 nm thick magnetic particles have been made by ion-milling Co, NiFe, and CoFe/Cu/NiFe films through tungsten masks made using self-assembled polystyrene-polyferrocenyldimethylsilane block copolymer templates. The arrays have 56 nm period and show short-range close-packed ordering in-plane. The particles have an in-plane easy axis, with substantial in-plane coercivity due to the effects of interactions and the distribution of grain size and particle shape. Reversal occurs by the collective switching of more than one particle, due to the strong interparticle magnetostatic interactions present in the arrays. Arrays made from CoFe/Cu/NiFe show antiparallel alignment between the layers as a result of magnetostatic coupling within the particles. These structures also exhibit a value of magnetoresistance which is similar to that of the unpatterned film, indicating that the ion-milling process preserves the layered structure even on this lateral length scale.

*Electronic address: caross@mit.edu

[1] J. I. Martin, J. Nogues, K. Liu, J. L. Vicente, and I. K. Schuller, J. Magn. Magn. Mater. **256**, 449 (2003).
[2] C. A. Ross, Ann. Rev. Mater. Res. **31**, 203 (2001).
[3] C. A. Ross, R. Chantrell, M. Hwang, M. Farhoud, T. A. Savas, Y. Hao, H. I. Smith, F. M. Ross, M. Redjdal, and F. B. Humphrey, Phys. Rev. B **62**, 14252 (2000).
[4] L. Néel, Ann. Geophys. (C.N.R.S.) **5**, 99 (1949).
[5] W. F. Brown, Phys. Rev. **130**, 1677 (1963).
[6] G. Meier, M. Kleiber, D. Grundler, D. Heitmann, and R. Wiesendanger, Appl. Phys. Lett. **72**, 2168 (1998).
[7] M. Hwang, M. Shima, C. A. Ross, C. Seberino, and H. N. Bertram, J. Appl. Phys. **92**, 1018 (2002).
[8] C. Haginoya, S. Heike, M. Ishibashi, K. Nakamura, K. Koike, T. Yoshimura, J. Yamanoto, and Y. Hirayami, J. Appl. Phys. **85**, 8327 (1999).
[9] R. M. H. New, R. F. W. Pease, and R. L. White, J. Magn. Magn. Mater. **155**, 140 (1996).
[10] G. Zheng, M. Pardavi-Horvath, and G. Vertesi, J. Appl. Phys. **81**, 5591 (1997).
[11] R. M. H. New, R. F. W. Pease, R. L. White, R. M. Osgood, and K. Babcock, J. Appl. Phys. **79**, 5851 (1996).
[12] J. Yu, U. Rudiger, L. Thomas, S. S. P. Parkin, and A. D. Kent, J. Appl. Phys. **85**, 5501 (1999).
[13] R. P. Cowburn, J. Phys. D **33**, R1 (2000).
[14] S. Evoy, D. W. Carr, L. Sekaric, Y. Suzuki, J. M. Parpia, and H. C. Craighead, J. Appl. Phys. **87**, 404 (2000).
[15] C. A. Ross, M. Hwang, M. Shima, J. Y. Cheng, M. Farhoud, T. A. Savas, H. I. Smith, W. Schwarzacher, F. M. Ross, M. Redjdal, and F. B. Humphrey, Phys. Rev. B **65**, 144417 (2002).
[16] A. Fernandez, M. R. Gibbons, M. A. Wall, and C. J. Cerjan, J. Magn. Magn. Mater. **190**, 71 (1998).
[17] M. A. M. Haast, J. R. Schuirhuis, L. Abelman, J. C. Lodder, and Th. J. Popma, IEEE Trans. Magn. **34**, 1006 (1998).
[18] G. Zangari and D. N. Lambeth, IEEE Trans. Magn. **33**, 3010 (1997).

[19] R. M. Metzger, V. V. Konovalov, M. Sun, T. Xu, G. Zangair, M. Benakli, and W. D. Doyle, IEEE Trans. Magn. **36**, 30 (2000).
[20] K. Nielsch, R. B. Wehrspohn, J. Barthel, J. Kirschner, U. Gösele, S. F. Fischer, and H. Kronmuller, Appl. Phys. Lett. **79**, 1360 (2001).
[21] X. Mei, M. Blumin, D. Kim, Z. Wu, and H. E. Ruda, J. Cryst. Growth **251**, 253 (2003).
[22] H. Masuda, K. Yasui, and K. Nishio, Adv. Mater. (Weinheim, Ger.) **12**, 1031 (2000).
[23] K. Liu, J. Nogues, C. Leighton, H. Masuda, K. Nishio, I. V. Roschin, and I. K. Schuller, Appl. Phys. Lett. **81**, 4434 (2002).
[24] S. P. Li, W. S. Lew, Y. B. Xu, A. Hirohata, A. Samad, F. Baker, and J. A. C. Bland, Appl. Phys. Lett. **76**, 748 (2000).
[25] T. Thurn-Albrecht, J. Schotter, G. A. Kastle, N. Emley, T. Shibauchi, L. Krusin-Elbaum, K. Guarini, C. T. Black, M. T. Tuominen, and T. P. Russell, Science **290**, 2126 (2000).
[26] K. Liu, S. M. Baker, M. Tuominen, T. P. Russell, and I. K. Schuller, Phys. Rev. B **63**, 060403R (2001).
[27] T. Shibauchi, L. Krusin-Elbaum, L. Gignac, C. T. Black, T. Thurn-Albrecht, T. P. Russell, J. Schotter, G. A. Kastle, N. Emley, and M. T. Tuominen, J. Magn. Magn. Mater. **226**, 1553 (2001).
[28] K. Shin, K. A. Leach, J. T. Goldbach, D. H. Kim, J. Y. Jho, M. Tuominen, C. J. Hawker, and T. P. Russell, Nano Lett. **2**, 933 (2002).
[29] R. R. Li, P. D. Dapkus, M. E. Thompson, W. G. Jeong, C. Harrison, P. M. Chaiken, R. A. Register, and D. H. Adamson, Appl. Phys. Lett. **76**, 1689 (2000).
[30] M. Bal, A. Ursache, M. Tuominen, J. T. Goldbach, and T. P. Russell, Appl. Phys. Lett. **81**, 3479 (2002).
[31] J. Y. Cheng, C. A. Ross, V. Z. Chan, E. L. Thomas, R. G. H. Lammertink, and G. J. Vancso, Adv. Mater. (Weinheim, Ger.) **13**, 1174 (2001).
[32] J. Y. Cheng, C. A. Ross, E. L. Thomas, H. I. Smith, and G. J. Vancso, IEEE Trans. Magn. **38**, 2541 (2002).
[33] K. Asakawa, T. Hiraoka, H. Hieda, M. Sakurai, and Y. Kamata, J. Photopolym. Sci. Technol. **15**, 465 (2002).
[34] K. Naito, H. Hieda, M. Sakurai, Y. Kamata, and K. Asakawa, IEEE Trans. Magn. **38**, 1949 (2002).
[35] C. T. Black, K. W. Guarini, K. R. Milkove, S. M. Baker, T. P. Russell, and M. T. Tuominen, Appl. Phys. Lett. **79**, 409 (2001).
[36] M. Park, P. M. Chaikin, R. A. Register, and D. H. Adamson, Appl. Phys. Lett. **79**, 257 (2001).
[37] S. Sun, C. B. Murray, D. Weller, L. Folks, and A. Moser, Science **287**, 1989 (2000).
[38] M. Park, C. Harrison, P. M. Chaikin, R. A. Register, and D. H. Adamson, Science **276**, 1401 (1997).
[39] J. Y. Cheng, C. A. Ross, E. L. Thomas, H. I. Smith, and G. J. Vancso, Appl. Phys. Lett. **81**, 3657 (2002).
[40] J. Y. Cheng, C. A. Ross, E. L. Thomas, H. I. Smith, and G. J. Vancso, Adv. Mater. (Weinheim, Ger.) **15**, 1599 (2003).
[41] R. A. Segalman, H. Yokohama, and E. J. Kramer, Adv. Mater. (Weinheim, Ger.) **13**, 1152 (2001).
[42] S. O. Kim, H. H. Solak, M. P. Stoykovich, N. J. Ferrier, J. J. de Pablo, and P. F. Nealey, Nature (London) **424**, 411 (2003).
[43] T. L. Morkved, M. Lu, A. M. Urbas, E. E. Ehrichs, H. M. Jaeger, P. Mansky, and T. P. Russell, Science **273**, 931 (1996).
[44] M. P. Sharrock, J. Appl. Phys. **76**, 6413 (1994).
[45] P. Bruno, G. Bayreuther, P. Beauvillain, C. Chappert, G. Lugert, D. Renard, J. P. Renard, and J. Seiden, J. Appl. Phys. **68**, 5759 (1990).
[46] P. L. Lu and S. H. Charap, J. Appl. Phys. **75**, 5768 (1994).
[47] Y. Hao, C. A. Ross, and H. I. Smith, J. Appl. Phys. **93**, 7909 (2003).
[48] O. Henkel, Phys. Status Solidi **7**, 191 (1964).
[49] G. Bottoni, D. Candolfo, and A. Ceccetti, J. Appl. Phys. **81**, 3809 (1997).
[50] A. Aharoni, J. Appl. Phys. **68**, 2892 (1990).
[51] K. Yu. Guslienko, S. B. Choe, and S. C. Shin, Appl. Phys. Lett. **76**, 3902 (2000).
[52] R. P. Cowburn, D. K. Koltsov, A. O. Adeyeye, M. E. Welland, and D. M. Tricker, Phys. Rev. Lett. **83**, 1042 (1999).
[53] H. Hoffmann and F. Steinbauer, J. Appl. Phys. **92**, 5463 (2002).
[54] A. J. Bennett and J. M. Xu, Appl. Phys. Lett. **82**, 2503 (2003).
[55] R. L. Stamps and R. E. Camley, Phys. Rev. B **60**, 11694 (1999).
[56] K. Yu. Guslienko, Appl. Phys. Lett. **75**, 394 (1999).
[57] D. Kechrakos and K. N. Trohidou, Appl. Phys. Lett. **81**, 4574 (2002).
[58] V. Russier, J. Appl. Phys. **89**, 1287 (2001).
[59] M. Schabes, J. Magn. Magn. Mater. **95**, 249 (1991).
[60] R. M. H. New, R. F. W. Pease, and R. L. White, IEEE Trans. Magn. **31**, 3805 (1995).
[61] Y. Zheng and J.-G. Zhu, J. Appl. Phys. **85**, 4776 (1999).
[62] F. J. Castano, Y. Hao, C. A. Ross, B. Vogeli, H. I. Smith, and S. Haratani, J. Appl. Phys. **91**, 7317 (2002).
[63] *Metals Handbook*, edited by H. E. Boyer and T. L. Gall (American Society for Metals, Metals Park, OH, 1985).
[64] F. J. Castano, S. Haratani, Y. Hao, C. A. Ross, and H. I. Smith, Appl. Phys. Lett. **81**, 2809 (2002).
[65] B. A. Everitt, A. V. Pohm, R. S. Beech, A. Fink, and J. M. Daughton, IEEE Trans. Magn. **34**, 1060 (1998).
[66] S. Parkin, X. Jiang, C. Kaiser, A. Panchula, K. Roche, and M. Samant, Proc. IEEE **91**, 661 (2003).